

pubs.acs.org/NanoLett Letter

A Generalized Approach to Photon Avalanche Upconversion in Luminescent Nanocrystals

Artiom Skripka,* Minji Lee, Xiao Qi, Jia-Ahn Pan, Haoran Yang, Changhwan Lee, P. James Schuck, Bruce E. Cohen, Daniel Jaque,* and Emory M. Chan*



Cite This: Nano Lett. 2023, 23, 7100-7106



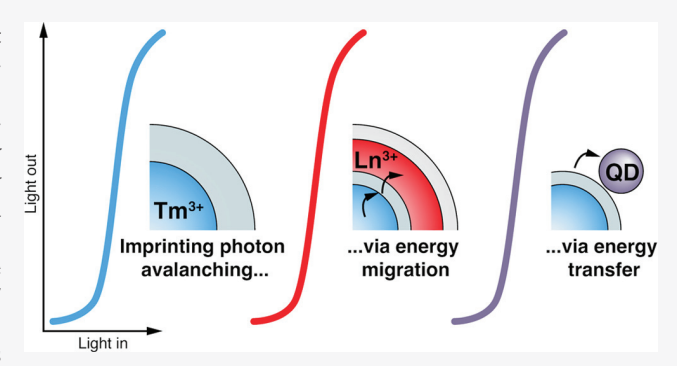
ACCESS

III Metrics & More

Article Recommendations

s Supporting Information

ABSTRACT: Photon avalanching nanoparticles (ANPs) exhibit extremely nonlinear upconverted emission valuable for subdiffraction imaging, nanoscale sensing, and optical computing. Avalanching has been demonstrated with Tm^{3+} -, Pr^{3+} -, or Nd^{3+} -doped nanocrystals, but their emission is limited to a few wavelengths and materials. Here, we utilize Gd^{3+} -assisted energy migration to tune the emission wavelengths of Tm^{3+} -sensitized ANPs and generate highly nonlinear emission from Eu^{3+} , Tb^{3+} , Ho^{3+} , and Er^{3+} ions. The upconversion intensities of these spectrally discrete ANPs scale with nonlinearity factor s = 10-17 under 1064 nm excitation at power densities as low as 7 kW cm⁻². This strategy for imprinting avalanche behavior on remote emitters can be extended to fluorophores adjacent to ANPs, as we



demonstrate with CdS/CdSe/CdS core/shell/shell quantum dots. ANPs with rationally designed energy transfer networks provide the means to transform conventional linear emitters into a highly nonlinear ones, expanding the use of photon avalanching in biological, chemical, and photonic applications.

KEYWORDS: upconversion, photon avalanche, spectral tuning, nonlinear emitters

hoton avalanching (PA) nanoparticles exhibit giant optical nonlinearities in their upconverted emission such that a 10-20% increase in near-infrared (NIR) excitation power can result in a 100-1000-fold increase in the emission intensity. PA behavior has been recently reported at room temperature in lanthanide (Ln3+)-doped nanocrystals of NaYF4:Tm3+,2 LiYF₄:Tm³⁺, KPb₂Cl₅:Nd³⁺, and NaYF₄:Yb³⁺, Pr^{3+,3-5} Their highly nonlinear responses, equivalent in some cases to those of >30-photon processes, have been utilized for nanoscale thermometers, for molecular rulers, and, most saliently, in subdiffraction microscopy⁶⁻¹⁰ to achieve optical resolutions finer than 100 nm using a conventional laser scanning microscope.² However, these early avalanching nanoparticles (ANPs) mostly emit in the NIR region (i.e., 800 nm), which limits the ability to probe multiple species independently at different visible wavelengths. To realize multiplexed applications of PA in imaging, sensing, and computing, ANPs with a broader wavelength range and spectrally distinct luminescence profiles must be developed.

To diversify the library of ANPs using the few proven PA compositions, we utilized energy migration to transfer the nonlinear behavior of the Ln³⁺ ions responsible for avalanching to physically segregated emitters within the same nanocrystals and also to neighboring nanoparticles. Similar energy migration upconversion (EMU) approaches have been used

in conventional upconverting nanoparticles (UCNPs) to tune upconversion with various $\rm Ln^{3+}$ emitters without changing underlying light sensitization mechanisms. 11,12 Such physical decoupling is even more essential for ANPs because the energy looping mechanism underpinning PA is particularly susceptible to quenching via cross-relaxation when additional ions are codoped with avalanching ions. In ANPs, energy migration through Yb³+ ions was recently used to transfer the avalanching behavior of the Yb³+/Pr³+ PA system to ions that emit at visible wavelengths (e.g., Tm³+ at 450 nm and Ho³+ at 540 and 650 nm). This approach, however, requires high excitation powers (>70 kW cm⁻²) and deconvolution of overlapping emission signals, and is restricted to a few select emitters.

Here, we demonstrate how PA originating from Tm^{3+} ions can be harnessed together with EMU through Gd^{3+} ions to create a library of spectrally discrete ANPs with low avalanching thresholds and highly nonlinear emissions (Figure 1). We posited that reducing the number of avalanching Tm^{3+}

Received: May 25, 2023 **Revised:** July 8, 2023 **Published:** July 20, 2023





Nano Letters pubs.acs.org/NanoLett Letter

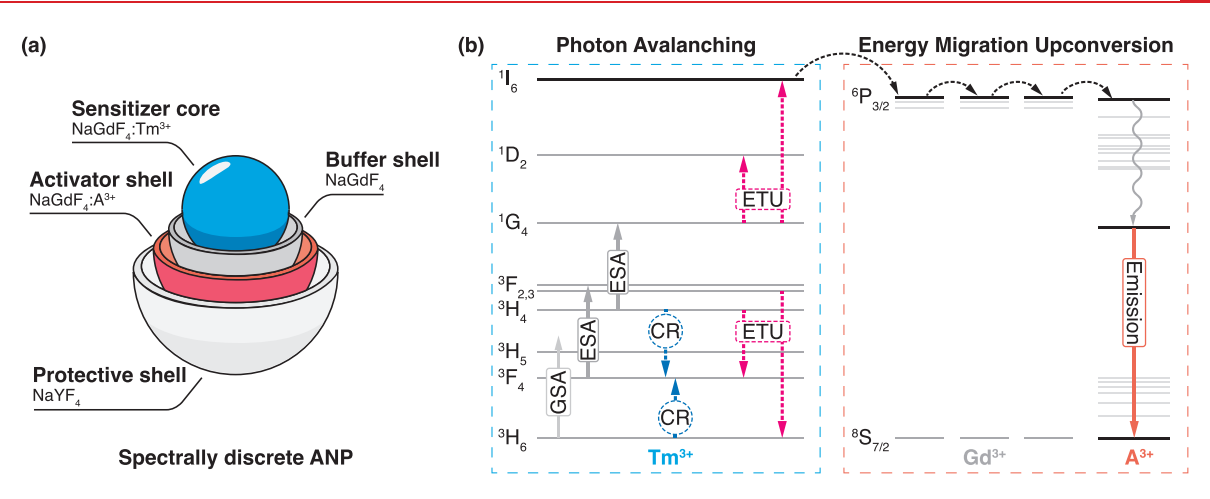


Figure 1. (a) Schematic representation of spectrally discrete ANPs consisting of the sensitizer core (NaGdF₄:Tm³⁺), buffer shell (NaGdF₄), activator shell (NaGdF₄:A³⁺), and protective shell (NaYF₄). (b) Simplified energy level diagram and operation of spectrally discrete ANPs depicting 1064 nm excited photon avalanche (GSA/ESA: ground/excited state absorption; CR: cross-relaxation; ETU: energy transfer upconversion), energy migration via Gd³⁺ ions, and instigation of visible avalanche upconversion in A³⁺ ions. Solid arrows: photon emission/absorption; dashed arrows: nonradiative energy transfer; wavy arrow: nonradiative multiphonon relaxation.

ions (<500) in small NaGdF₄ core nanoparticles (<7 nm) would accelerate saturation of the ³H₄ state and facilitate population of higher-energy levels of Tm³⁺ (¹D₂ and ¹I₆).^{8,13} Subsequently, energy from these excited Tm3+ ions can be transferred to Gd3+ ions in the host matrix and relayed to any activator lanthanide ion (A³⁺) in a nanocrystal. Because the energy of Gd³⁺ ions (⁶P_I) is transferred from Tm³⁺ ions excited by multiple stages of PA, the high nonlinearity of PA can be preserved in the emission of A³⁺ ions (Figure 1b). Furthermore, EMU in ANPs can be extended to semiconductor quantum dots (QD), prompting highly nonlinear emission from ANP+QD avalanching composites. Such avalanching composites could enable development of longrange energy transfer sensors with high localization precision. Overall, the combination of Tm³⁺-PA and Gd³⁺-EMU provides a way to easily customize the upconversion emission of ANPs. The spectrally discrete ANPs and avalanching composites demonstrated here enrich the palette of available nonlinear emitters for a range of photonic applications.

To implement this EMU photon avalanching architecture, we synthesized heterostructured ANPs consisting of a NaGdF₄:20 mol % Tm³⁺ sensitizer core, an undoped NaGdF₄ buffer shell, a NaGdF₄:15 mol % Eu³⁺ activator shell, and an undoped NaYF₄ outer shell (Figure 2a,b). Each shell of ANPs was grown sequentially by thermal decomposition of precursors using a nanoparticle synthesis robot, WANDA (see Section S1 in the Supporting Information for synthesis details). 14,15 We found excellent agreement between the shelling injection cycles and nanocrystal size increase after deposition of each shell, accurate within one monolayer (0.48 nm; Figure 2a and Tables S1, S2). An intermediate NaGdF₄ buffer shell was introduced to minimize direct energy transfer between sensitizer (Tm³+) and activator (Eu³+) ions, which could lead to quenching. ¹⁶ Meanwhile, the protective NaYF₄ outer shell (Figure S1 shows elemental mapping of Gd3+ and Y3+ ions) was used to reduce surface quenching and prevent excitation energy spill-out from the Gd3+ network. 17,18 As synthesized, the Eu3+-activated ANPs were observed to be a pure Na(Y/Gd)F₄ β -phase (Figure S2) and less than 25 nm in diameter, determined by powder X-ray diffraction (XRD) and transmission electron microscopy (TEM), respectively. High

crystallinity, small size, and narrow size distribution (<5%) ideally position these ANPs for biological or nanoscale patterning applications. ^{19–21}

Under 1064 nm irradiation the Eu³+-activated ANPs emitted 800 nm light characteristic of $^3{\rm H}_4 \rightarrow ^3{\rm H}_6$ radiative relaxation in avalanching Tm³+ ions (Figure S3).²-14 Interestingly, we observed a series of visible emission peaks at 510, 535, 555, 580, 590, and 615 nm, consistent with Eu³+ radiative transitions from the $^5{\rm D}_J$ excited states (Figure 2c). The presence of Eu³+ emission confirms that energy migration from the Tm³+-doped core to the Eu³+-doped shell occurs through the Gd³+ sublattice, especially because no emission was detected with Tm³+-free core/shell NaGdF4:15 mol % Eu³+/NaYF4 control nanoparticles excited at 1064 nm (Figure S7). We note that the emission profile of Eu³+ in the 500–640 nm range has no overlap with that of Tm³+ upconversion and can be readily detected without the need for spectral deconvolution.

To determine whether PA occurs in these Eu³⁺-activated ANPs, we investigated the power dependence of the visible Eu³⁺ and NIR Tm³⁺ emissions (Figure 2d; power-dependent spectra shown in Figure S3). With pump power (P) increasing above the 16 kW cm⁻² threshold, the intensity (I) of the Tm³ $(^{3}H_{4} \rightarrow ^{3}H_{6})$ line at 800 nm increased with the nonlinearity factor s = 15.1, where s is the slope of the log-log plot in Figure 2d, and $I \propto P^s$. Further increasing the power above 30 kW cm⁻², we observed power-dependent scaling of the Eu³⁺ $(^{5}D_{0} \rightarrow {}^{7}F_{2})$ line at 615 nm with s = 14.6 (13.4 ± 2.1 from three independent measurements). This steep power scaling of Eu³⁺ emission (i.e., s > 10) strongly suggests that the nonlinear behavior of the avalanching Tm³⁺ core is preserved in highenergy states (e.g., ¹I₆) and can be transferred to Eu³⁺ ions by Gd³⁺-facilitated energy migration. Notably, Tm³⁺ excitation to the 1I6 energy state introduces additional energy transfer upconversion, cross-relaxation, and energy loss pathways, which shift the threshold for Eu³⁺ emission to greater pump powers. As an additional indication of PA in Eu³⁺-activated ANPs, we observed prolonged rise times in time-resolved Eu³⁺ luminescence and their subsequent shortening with the increasing pump power (Figure S4), both of which are signatures of PA.

Nano Letters pubs.acs.org/NanoLett Letter

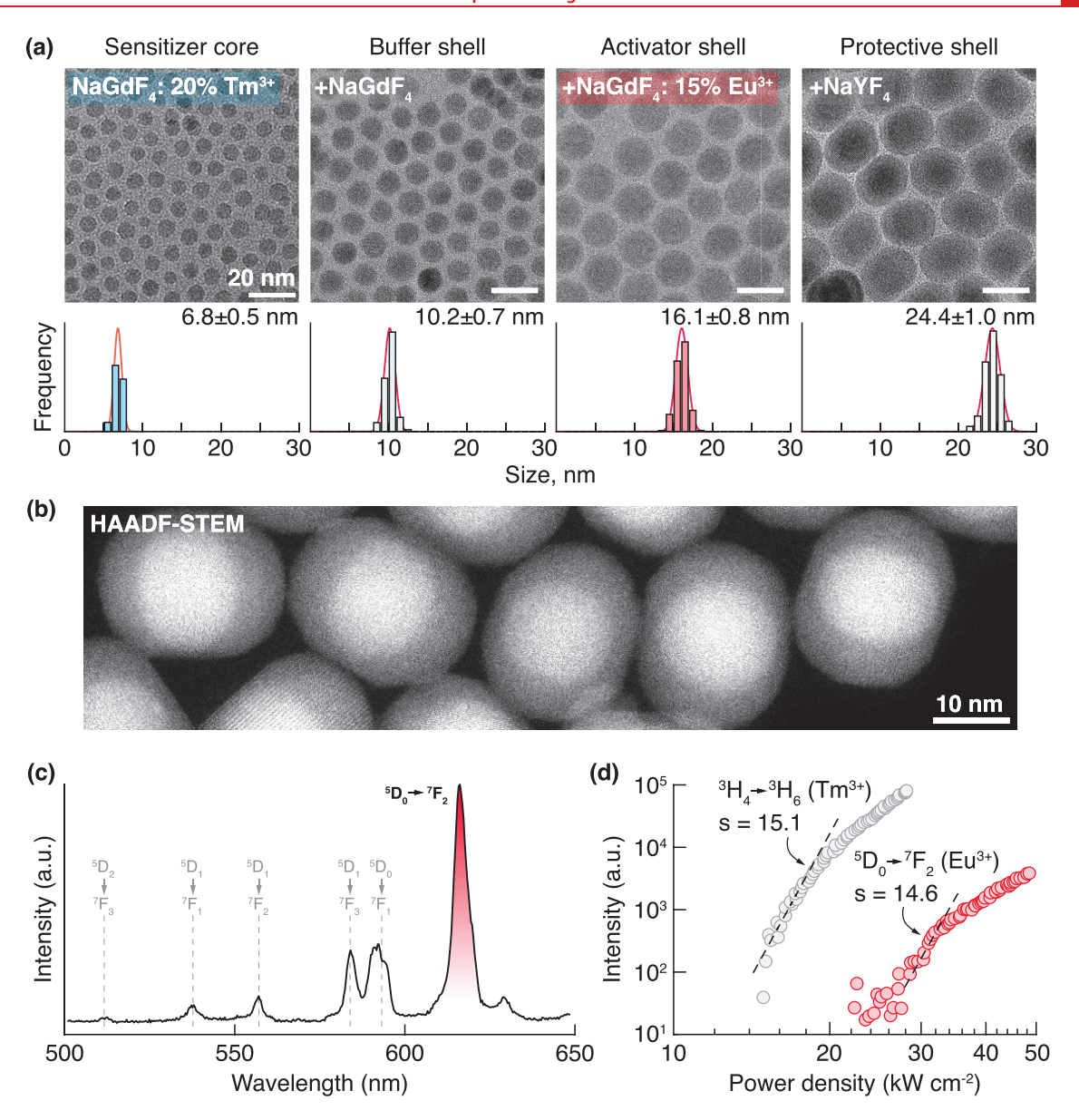


Figure 2. (a) Representative TEM micrographs of NaGdF₄:20% Tm³⁺/NaGdF₄/NaGdF₄:15% Eu³⁺/NaYF₄ ANPs following each synthesis step. Scale bar: 20 nm. Corresponding nanoparticle size distribution histograms together with average size and one standard size deviation are shown below each micrograph. (b) High-angle angular dark-field scanning transmission electron microscopy (HAADF-STEM) image of Eu³⁺-activated ANPs. (c) Eu³⁺ upconversion emission spectra in ANPs under 1064 nm excitation (49 kW cm⁻²). The identified Eu³⁺ transitions are labeled next to each band. (d) Pump power dependence of Eu³⁺ [5 D₀ \rightarrow 7 F₂; red circles; red highlight in (c)] and Tm³⁺ (3 H₄ \rightarrow 3 H₆; gray circles) emission under 1064 nm excitation. Steepest intensity scaling of Eu³⁺ emission with a nonlinearity factor s = 14.6 is derived from a linear fit of the log–log plot; Tm³⁺ emission scales with s = 15.1.

After establishing that EMU in ANPs can generate Eu³⁺ emission with high nonlinearity, we sought to corroborate the importance of energy migration within the Gd³⁺ network. To probe energy relay from the sensitizing Tm³⁺ core to the Eu³⁺ activator shell, we prepared a series of core/multishell NaGdF₄:20 mol % Tm³⁺/NaY_{1-x}Gd_xF₄/NaGdF₄:15 mol % Eu³⁺/NaYF₄ ANPs in which the amount of Gd³⁺ in the intermediate buffer shell was varied (x = 0.0, 0.2, 0.4, 1.0) (see Section S4 in the Supporting Information). When no Gd³⁺ was present in the buffer shell (x = 0), energy transfer was suppressed and Tm³⁺ visible upconversion (including $^{1}D_{2} \rightarrow ^{3}H_{5}$ transition at 510 nm) dominated the spectrum (Figure 3a, gray spectrum). When we introduced Gd³⁺ ions into the buffer shell (x = 0.2-1.0), Eu³⁺ upconversion at 510 nm ($^{5}D_{2} \rightarrow ^{7}F_{3}$)

could be observed. The intensity of this Eu³+ emission line increased relative to that of the Tm³+ line at 450 nm ($^1D_2 \rightarrow ^3F_4$) with increasing Gd³+ concentration with the maximum Eu³+ emission intensity observed for the case of a NaGdF₄ buffer shell (Figure 3a, red spectrum). We were also able to measure steeply nonlinear Eu³+ emission in NaGdF₄:20 mol % Tm³+/NaGdF₄:15 mol % Eu³+/NaYF₄ ANPs without the intermediate buffer shell (Section S5 in the Supporting Information); however, 2 orders of magnitude greater laser power was required (gray data points in Figure 3b). In contrast, Tm³+ NIR emission ($^3H_4 \rightarrow ^3H_6$) was observed with these ANPs at significantly lower powers (Figure S15), suggesting that Eu³+ quenches the higher energy states of Tm³+ (1G_4 and 1D_2) that do not participate in $^3H_4 \rightarrow ^3H_6$ PA

Nano Letters pubs.acs.org/NanoLett Lette

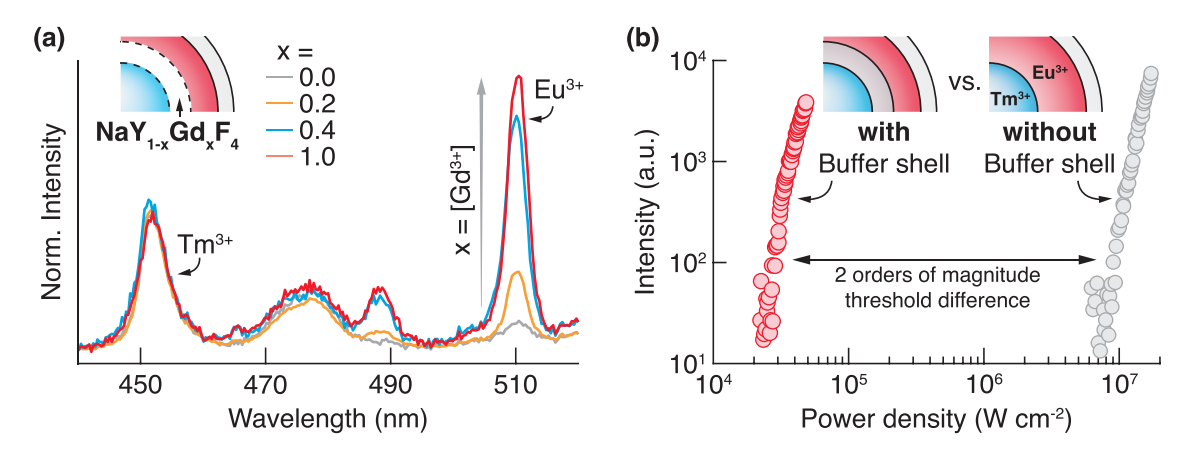


Figure 3. (a) Upconversion luminescence spectra of Eu^{3+} -activated ANPs with varying amounts of Gd^{3+} in the $NaY_{1-x}Gd_xF_4$ buffer shell (x=0.0, 0.2, 0.4, 1.0). Spectra are normalized to the Tm^{3+} emission intensity at 450 nm ($^1D_2 \rightarrow ^3F_4$). Spectra were acquired with 190 kW cm $^{-2}$ laser excitation power density to accentuate visible Tm^{3+} upconversion. (b) Pump power dependence of Eu^{3+} upconversion under 1064 nm excitation in ANPs with (red circles) and without (gray circles) NaGdF₄ buffer shell. Two orders of magnitude greater pump powers are required to promote nonlinear Eu^{3+} emission in ANPs without the buffer shell.

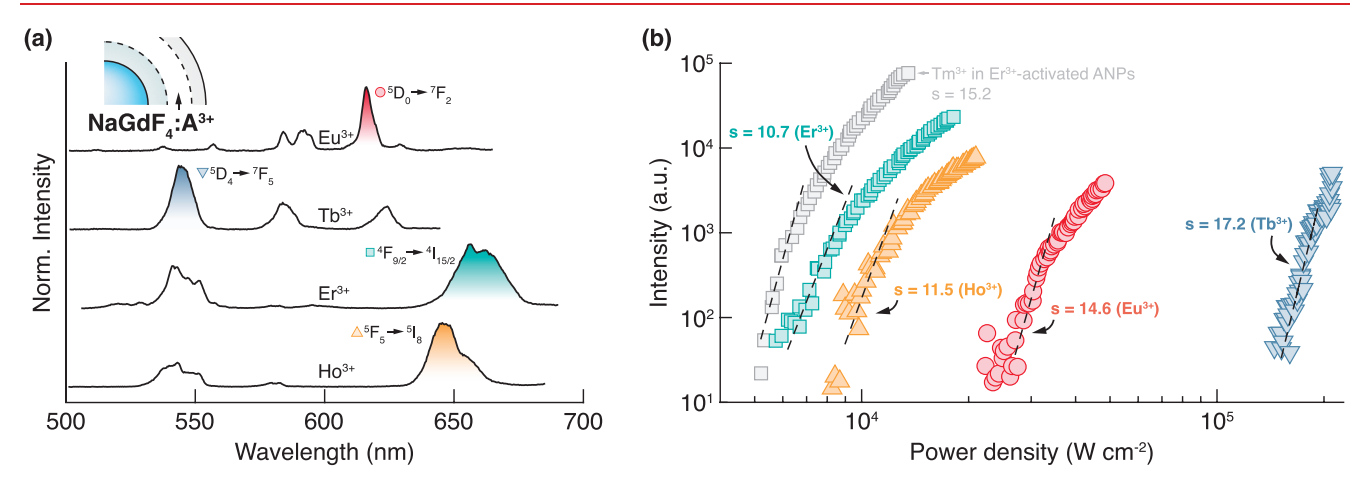


Figure 4. (a) Upconversion emission spectra in the 500–700 nm range of spectrally discrete ANPs containing different A^{3+} ions (Eu³⁺, Tb³⁺, Er³⁺, or Ho³⁺) in the activator shell under 1064 nm excitation. Spectra of Eu³⁺-, Er³⁺-, and Ho³⁺-activated ANPs were taken at 49 kW cm⁻² laser power density, and that of Tb³⁺-activated ANPs was taken at 580 kW cm⁻². (b) Pump power dependence of A^{3+} emission [shaded bands in (a)] intensities under 1064 nm excitation. Intensity scaling with representative nonlinearity factors s = 10-17 is derived from a linear fit of the log–log plot. Pump power dependence of Tm³⁺ NIR emission (${}^{3}H_{4} \rightarrow {}^{3}H_{6}$) in Er³⁺-activated ANPs is also shown (gray squares). Power scaling of Tm³⁺-PA emission in other spectrally discrete ANPs is shown in Figure S30.

emission. The above observations reinforce the importance of the NaGdF $_4$ buffer shell for preventing direct ${\rm Tm}^{3+}{\rm -Eu}^{3+}$ energy crosstalk while preserving EMU. As a further benefit, the buffer shell provides additional passivation of ${\rm Tm}^{3+}$ core from surface quenching. 22,23

Following the demonstration of remote PA in Eu³⁺-activated ANPs, we sought to extend this strategy to other A³⁺ ions to provide a generalized approach for the spectral tuning of extreme nonlinearities. We prepared a library of ANPs with Tm³⁺-doped cores and activator shells doped with Tb³⁺, Er³⁺, Ho³⁺, Nd³⁺, or Dy³⁺ ions. These core/multishell ANPs share the same NaGdF₄:Tm³⁺ sensitizer core, NaGdF₄ intermediate buffer shell, and NaYF₄ outer protective shell (as in the Eu³⁺-activated ANPs shown in Figure 1a)—only the composition of the activator (NaGdF₄:A³⁺) shell is changed. The above ANPs were observed to have a pure β -phase and diameters smaller than 25 nm (see Section S6 in the Supporting Information). Under 1064 nm excitation, each composition of ANPs featured a unique spectral profile of the selected A³⁺ ion in the visible

spectrum (Figures 4a and S26). We note that due to low upconversion intensity and unforeseen contamination by Er³⁺ ions, Nd3+- and Dy3+-activated ANPs were omitted from further studies. To validate that upconversion in other spectrally discrete ANPs stems from PA and EMU, we irradiated Tm3+-free NaGdF4:2 mol % Er3+/NaYF4 control nanoparticles with 1064 nm excitation (Figure S29a, which also shows emission at resonant 980 nm excitation). Er³⁺ upconversion was only detected at laser power densities greater than 1 MW cm⁻², and its power dependence (s = 1.8) followed a two-photon process (Figure S29b). In contrast, emission from different A3+ ions in spectrally discrete ANPs was generated in a highly nonlinear fashion, with representative (average \pm s.d.) nonlinearity factors s of 17.2 (14.9 \pm 2.6), 11.5 (10.4 \pm 1.1), and 10.7 (9.4 \pm 1.4) observed for Tb³⁺-, Ho³⁺-, and Er³⁺-activated ANPs, respectively (Figure 4b).

Notably, power densities as low as 7 and 10 kW cm $^{-2}$ were enough to promote visible PA upconversion from Er $^{3+}$ - and Ho $^{3+}$ -activated ANPs, respectively, similar to those originally

Nano Letters pubs.acs.org/NanoLett Letter

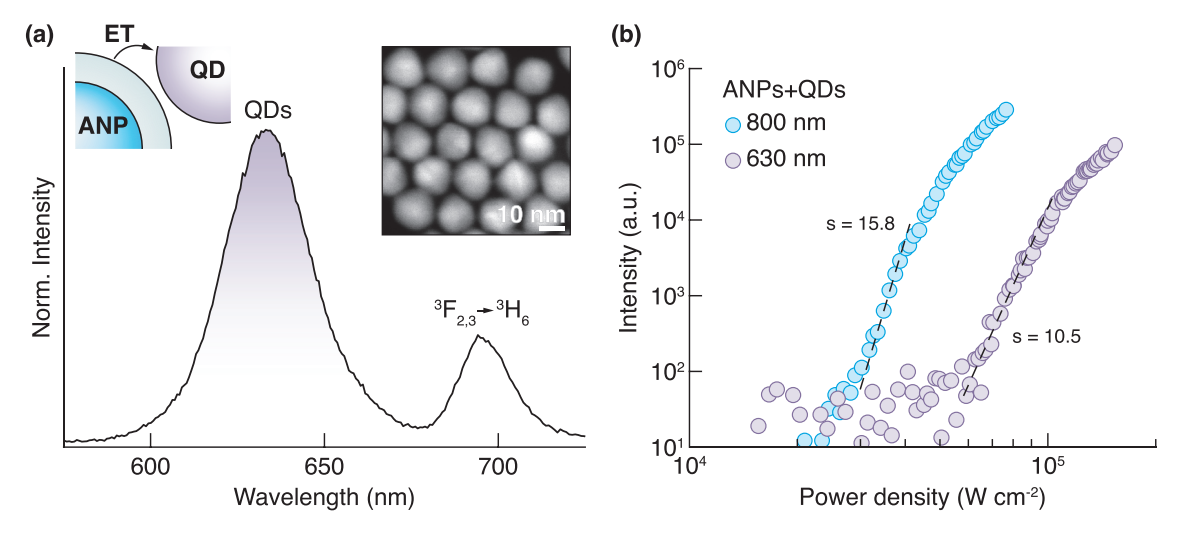


Figure 5. (a) Upconversion emission spectra of codeposited NaGdF₄: $Tm^{3+}/NaGdF_4$ ANPs and CdS/CdSe/CdS QDs under 1064 nm excitation (100 kW cm⁻²). ET is energy transfer. Inset: HAADF-STEM image of QDs; scale bar = 10 nm. (b) Pump power dependence of ANP (Tm^{3+} at 800 nm; blue circles) and QD (630 nm as highlighted in (a); purple circles) emission intensities under 1064 nm excitation. The steepest intensity scaling and corresponding nonlinearity factors (shown in the figure) are derived from a linear fit of the log-log plot.

reported for NaYF₄:Tm³⁺/NaYF₄:Gd³⁺ ANPs² and substantially lower than other ANPs.⁵ In generating A³⁺ emission across spectrally discrete ANPs, we observed some variation of the excitation power density threshold, with the lowest for Er3+-activated ANPs and the highest for Tb3+-activated ANPs (>160 kW cm⁻², Figure 4b). This difference could not be attributed to the underlying Tm3+-PA mechanism because the power threshold for 800 nm PA emission was similar across different ANPs (Figures S30 and 4b, gray points). We speculate that these discrepancies arise from small fluctuations in the thickness of the buffer NaGdF4 and protective NaYF4 shells as well as possible Tm3+ and A3+ dopant intermixing in the buffer shell.²⁴ The PA power threshold increases when energy can be directly passed between Tm3+ and A3+ ions (Figure 3b) and is highly sensitive to surface quenchers.²³ Additionally, powers above 100 kW cm⁻² can lead to photodarkening of Tm³⁺-based ANPs,⁸ which quenches emission during measurements and shifts the PA threshold to higher powers. Notwithstanding the power threshold differences, we can generalize that EMU spectral tuning can be adopted in ANPs for generating highly nonlinear emission (s > 10) from virtually any activator ion by the Tm³⁺ \rightarrow Gd³⁺ \rightarrow A³⁺ energy transfer cascade (Figure 1b; the mechanism of Tm³⁺ excitation to ¹I₆ was informed by numerical simulations; see Section S9 in the Supporting Information for details).

Inspired by the above results, we sought to demonstrate how EMU can facilitate PA-like nonlinear excitation of external fluorophores. To demonstrate this concept, we optically characterized a mixture of core/shell NaGdF₄:20 mol % Tm³⁺/NaGdF₄ ANPs and core/multishell CdS/CdSe/CdS quantum dots (QDs) codeposited on a glass coverslip (see Section S10 in the Supporting Information for details). Under 1064 nm excitation, the photoluminescence of both ANPs and QDs could be directly observed (Figure 5a). ANP emission stemmed primarily from the 3 H₄ \rightarrow 3 H₆ transition of Tm³⁺ ions at 800 nm, and a weaker band at 690 nm (3 F_{2,3} \rightarrow 3 H₆) could be observed at high excitation powers. Importantly, this Tm³⁺ emission had minimal overlap with the QD emission observed at 630 nm (Figure S36b). Although the QDs alone could be excited with a 1064 nm laser via two-photon

excitation (TPE; Figure S36c), in the presence of ANPs their emission intensity increased beyond the quadratic scaling observed without ANPs (Figure S37a). The excitation of QDs by ANP \rightarrow QD energy transfer resulted in QD emission power dependence with s=10.5 (purple circles in Figure Sb; the background signal of QD photoluminescence by direct 1064 nm excitation was subtracted from raw data prior to log–log plot fitting). The PA emission of ANPs (blue circles in Figure Sb) in the ANP + QD mixture had a lower power threshold and a higher degree of nonlinearity (s=15.8), as expected because energy transfer to QDs requires ANP excitation into high-energy states and introduces additional relaxation pathways. These experiments corroborate the involvement of the Tm³⁺ \rightarrow Gd³⁺ \rightarrow QDs energy transfer cascade at around 70 kW cm⁻² (for the present combination of nanoparticles).

To examine if QD activation happens via energy transfer from the Gd3+ ions in the ANP shells, we optically characterized ANPs that lacked Gd3+ ions in their shells (i.e., NaGdF₄:20% Tm³⁺/NaYF₄). We hypothesized that the resulting suppression of energy migration to ANP surfaces would minimize nonradiative energy transfer to QDs due to the longer Ln³⁺-QD distances. For the NaGdF₄:Tm³⁺/NaYF₄ ANPs + QD mixture excited above 100 kW cm⁻², the degree of nonlinearity was significantly lower (s = 6.7, Figure S37b) than when EMU was allowed (Figure 5b), although the power dependence was still greater than the quadratic power scaling expected for TPE of QDs. We speculate that in the absence of Gd3+ ions in the shell, radiative energy transfer from ANPs to QDs can occur and increase the nonlinearity of QD photoluminescence at high excitation powers. Conversely, in ANPs with Gd³⁺ sublattices that extend to their surfaces (i.e., NaGdF₄:Tm³⁺/NaGdF₄), both radiative and nonradiative $(Gd^{3+} \rightarrow QDs)$ interparticle energy transfer can take place. However, further experimental studies are required to better understand energy transfer from ANPs as energy donors. Altogether, we successfully extended PA from ANPs to other fluorophores via interparticle EMU, demonstrating the ability to form avalanching composites for highly sensitive multiplexing and subdiffraction imaging assays.²⁶,

In summary, we demonstrate that the combination of Tm³⁺based PA and Gd³⁺-assisted EMU is an effective approach to tune the emission spectra of photon avalanching nanoparticles. Using spectrally discrete ANPs, upconversion profiles of Er³⁺ Ho³⁺, Eu³⁺, Nd³⁺, Dy³⁺, and Tb³⁺ were observed under 1064 nm excitation with highly nonlinear intensity power scaling (s = 10-17). Through rational design of the heterostructured ANPs, PA emission of activators was generated in nanocrystals as small as 25 nm in diameter and at exceptionally low laser excitation power densities ($\leq 10 \text{ kW cm}^{-2}$). Importantly, we found that PA can be extended beyond lanthanide ions, as demonstrated by PA-like emission of semiconductor QDs in ANP+QD avalanching composites, which showcases how extreme nonlinearities can be imprinted onto linear emitters. We believe that these findings represent a significant step forward in developing ANPs with customizable compositions, tunable photoluminescence properties, and synergistic interaction with other fluorophores, with potential application in multicolor subdiffraction imaging, surface patterning, and ultrasensitive bioassays.

METHODS

Detailed information regarding nanoparticle synthesis and structural and spectroscopic characterization is provided in the Supporting Information.

ASSOCIATED CONTENT

Supporting Information

The Supporting Information is available free of charge at https://pubs.acs.org/doi/10.1021/acs.nanolett.3c01955.

Complete ANP and QD synthesis and characterization description; additional XRD, TEM, photoluminescence, and simulation data, including Scheme 1, Figures S1–S37, Tables S1–S6 (PDF)

AUTHOR INFORMATION

Corresponding Authors

Artiom Skripka — The Molecular Foundry, Lawrence Berkeley National Laboratory, Berkeley, California 94720, United States; Nanomaterials for Bioimaging Group, Departamento de Física de Materiales, Facultad de Ciencias, Universidad Autónoma de Madrid, Madrid 28049, Spain; orcid.org/0000-0003-4060-4290; Email: a skripka@lbl.gov

Daniel Jaque — Nanomaterials for Bioimaging Group,
Departamento de Física de Materiales, Facultad de Ciencias
and Institute for Advanced Research in Chemical Sciences
(IAdChem), Universidad Autónoma de Madrid, Madrid
28049, Spain; orcid.org/0000-0002-3225-0667;
Email: daniel.jaque@uam.es

Emory M. Chan — The Molecular Foundry, Lawrence Berkeley National Laboratory, Berkeley, California 94720, United States; orcid.org/0000-0002-5655-0146; Email: emchan@lbl.gov

Authors

Minji Lee – The Molecular Foundry, Lawrence Berkeley National Laboratory, Berkeley, California 94720, United States; Department of Chemical and Biomolecular Engineering, University of California, Berkeley, Berkeley, California 94720, United States

- Xiao Qi The Molecular Foundry, Lawrence Berkeley National Laboratory, Berkeley, California 94720, United States
- Jia-Ahn Pan The Molecular Foundry and Chemical Science Division, Lawrence Berkeley National Laboratory, Berkeley, California 94720, United States; ⊚ orcid.org/0000-0001-6153-8611
- Haoran Yang The Molecular Foundry, Lawrence Berkeley National Laboratory, Berkeley, California 94720, United States; Occid.org/0000-0002-9709-1062
- Changhwan Lee Department of Mechanical Engineering, Columbia University, New York, New York 10027, United States
- P. James Schuck Department of Mechanical Engineering, Columbia University, New York, New York 10027, United States; orcid.org/0000-0001-9244-2671
- Bruce E. Cohen The Molecular Foundry, Lawrence Berkeley National Laboratory, Berkeley, California 94720, United States; Division of Molecular Biophysics & Integrated Bioimaging, Lawrence Berkeley National Laboratory, Berkeley, California 94720, United States; orcid.org/ 0000-0003-3655-3638

Complete contact information is available at: https://pubs.acs.org/10.1021/acs.nanolett.3c01955

Notes

The authors declare no competing financial interest.

■ ACKNOWLEDGMENTS

A.S. acknowledges support from the European Union's Horizon 2020 research and innovation program under the Marie Skłodowska-Curie Grant Agreement No. 895809 (MONOCLE). Work at the Molecular Foundry was supported by the U.S. Department of Energy (DOE) under Contract DE-AC02-05CH11231 through the Office of Science, Office of Basic Energy Sciences and J.A. through the Chemical Sciences, Geosciences, and Biosciences Division, Separations Program. H.Y. and quantum dot synthesis were supported by the DOE Office of Energy Efficiency and Renewable Energy (EERE), under Award DE-EE0007628. X.Q., B.E.C., and E.M.C. were supported by the Defense Advanced Research Projects Agency (DARPA) under Contract HR0011257070. C.L. and P.J.S. acknowledge support from DARPA Contract HR00112220006 and from the National Science Foundation Grant CHE-2203510. This work was financed by the Spanish Ministerio de Innovación y Ciencias under Project NANONERV PID2019-106211RB-I00 and by the Comunidad Autónoma de Madrid (S2022/BMD-7403 RENIM-CM).

■ REFERENCES

- (1) Joubert, M.-F. Photon Avalanche Upconversion in Rare Earth Laser Materials. *Opt. Mater.* **1999**, *11* (2–3), 181–203.
- (2) Lee, C.; Xu, E. Z.; Liu, Y.; Teitelboim, A.; Yao, K.; Fernandez-Bravo, A.; Kotulska, A. M.; Nam, S. H.; Suh, Y. D.; Bednarkiewicz, A.; Cohen, B. E.; Chan, E. M.; Schuck, P. J. Giant Nonlinear Optical Responses from Photon-Avalanching Nanoparticles. *Nature* **2021**, *589* (7841), 230–235.
- (3) Dudek, M.; Szalkowski, M.; Misiak, M.; Ćwierzona, M.; Skripka, A.; Korczak, Z.; Piątkowski, D.; Woźniak, P.; Lisiecki, R.; Goldner, P.; Maćkowski, S.; Chan, E. M.; Schuck, P. J.; Bednarkiewicz, A. Size-Dependent Photon Avalanching in Tm³⁺ Doped LiYF₄ Nano, Micro, and Bulk Crystals. *Adv. Opt. Mater.* **2022**, *10*, 2201052.

- (4) Zhang, Z.; Skripka, A.; Dahl, J. C.; Dun, C.; Urban, J. J.; Jaque, D.; Schuck, P. J.; Cohen, B. E.; Chan, E. M. Tuning Phonon Energies in Lanthanide-doped Potassium Lead Halide Nanocrystals for Enhanced Nonlinearity and Upconversion. *Angew. Chem., Int. Ed.* **2023**, 62 (1), e202212549.
- (5) Liang, Y.; Zhu, Z.; Qiao, S.; Guo, X.; Pu, R.; Tang, H.; Liu, H.; Dong, H.; Peng, T.; Sun, L.-D.; Widengren, J.; Zhan, Q. Migrating Photon Avalanche in Different Emitters at the Nanoscale Enables 46th-Order Optical Nonlinearity. *Nat. Nanotechnol.* **2022**, *17* (5), 524–530.
- (6) Denkova, D.; Ploschner, M.; Das, M.; Parker, L. M.; Zheng, X.; Lu, Y.; Orth, A.; Packer, N. H.; Piper, J. A. 3D Sub-Diffraction Imaging in a Conventional Confocal Configuration by Exploiting Super-Linear Emitters. *Nat. Commun.* **2019**, *10* (1), 3695.
- (7) Bednarkiewicz, A.; Chan, E. M.; Kotulska, A.; Marciniak, L.; Prorok, K. Photon Avalanche in Lanthanide Doped Nanoparticles for Biomedical Applications: Super-Resolution Imaging. *Nanoscale Horiz* **2019**, *4* (4), 881–889.
- (8) Lee, C.; Xu, E. Z.; Kwock, K. W. C.; Teitelboim, A.; Liu, Y.; Park, H. S.; Ursprung, B.; Ziffer, M. E.; Karube, Y.; Fardian-Melamed, N.; Pedroso, C. C. S.; Kim, J.; Pritzl, S. D.; Nam, S. H.; Lohmueller, T.; Owen, J. S.; Ercius, P.; Suh, Y. D.; Cohen, B. E.; Chan, E. M.; Schuck, P. J. Indefinite and Bidirectional Near-Infrared Nanocrystal Photoswitching. *Nature* **2023**, *618* (7967), 951–958.
- (9) Bednarkiewicz, A.; Chan, E. M.; Prorok, K. Enhancing FRET Biosensing beyond 10 Nm with Photon Avalanche Nanoparticles. *Nanoscale Adv.* **2020**, 2 (10), 4863–4872.
- (10) Szalkowski, M.; Dudek, M.; Korczak, Z.; Lee, C.; Marciniak, Ł.; Chan, E. M.; Schuck, P. J.; Bednarkiewicz, A. Predicting the Impact of Temperature Dependent Multi-Phonon Relaxation Processes on the Photon Avalanche Behavior in Tm³⁺: NaYF₄ Nanoparticles. *Opt. Mater.: X* **2021**, *12*, 100102.
- (11) Wang, F.; Deng, R.; Wang, J.; Wang, Q.; Han, Y.; Zhu, H.; Chen, X.; Liu, X. Tuning Upconversion through Energy Migration in Core–Shell Nanoparticles. *Nat. Mater.* **2011**, *10* (12), 968–973.
- (12) Guo, X.; Pu, R.; Zhu, Z.; Qiao, S.; Liang, Y.; Huang, B.; Liu, H.; Labrador-Páez, L.; Kostiv, U.; Zhao, P.; Wu, Q.; Widengren, J.; Zhan, Q. Achieving Low-Power Single-Wavelength-Pair Nanoscopy with NIR-II Continuous-Wave Laser for Multi-Chromatic Probes. *Nat. Commun.* 2022, 13 (1), 2843.
- (13) Xu, E. Z.; Lee, C.; Pritzl, S. D.; Chen, A. S.; Lohmueller, T.; Cohen, B. E.; Chan, E. M.; Schuck, P. J. Infrared-to-Ultraviolet Upconverting Nanoparticles for COVID-19-Related Disinfection Applications. *Opt. Mater.: X* **2021**, *12*, 100099.
- (14) Levy, E. S.; Tajon, C. A.; Bischof, T. S.; Iafrati, J.; Fernandez-Bravo, A.; Garfield, D. J.; Chamanzar, M.; Maharbiz, M. M.; Sohal, V. S.; Schuck, P. J.; Cohen, B. E.; Chan, E. M. Energy-Looping Nanoparticles: Harnessing Excited-State Absorption for Deep-Tissue Imaging. ACS Nano 2016, 10 (9), 8423–8433.
- (15) Chan, E. M.; Xu, C.; Mao, A. W.; Han, G.; Owen, J. S.; Cohen, B. E.; Milliron, D. J. Reproducible, High-Throughput Synthesis of Colloidal Nanocrystals for Optimization in Multidimensional Parameter Space. *Nano Lett.* **2010**, *10* (5), 1874–1885.
- (16) Wang, X.; Yan, L.; Liu, S.; Zhang, P.; Huang, R.; Zhou, B. Enhancing Energy Migration Upconversion through a Migratory Interlayer in the Core–Shell–Shell Nanostructure towards Latent Fingerprinting. *Nanoscale* **2020**, *12* (36), 18807–18814.
- (17) Su, Q.; Han, S.; Xie, X.; Zhu, H.; Chen, H.; Chen, C.-K.; Liu, R.-S.; Chen, X.; Wang, F.; Liu, X. The Effect of Surface Coating on Energy Migration-Mediated Upconversion. *J. Am. Chem. Soc.* **2012**, 134 (51), 20849–20857.
- (18) Pu, R.; Zhan, Q.; Peng, X.; Liu, S.; Guo, X.; Liang, L.; Qin, X.; Zhao, Z. W.; Liu, X. Super-Resolution Microscopy Enabled by High-Efficiency Surface-Migration Emission Depletion. *Nat. Commun.* **2022**, *13* (1), 6636.
- (19) Pedroso, C. C. S.; Mann, V. R.; Zuberbühler, K.; Bohn, M.-F.; Yu, J.; Altoe, V.; Craik, C. S.; Cohen, B. E. Immunotargeting of Nanocrystals by SpyCatcher Conjugation of Engineered Antibodies. *ACS Nano* **2021**, *15* (11), 18374–18384.

- (20) Voronovic, E.; Skripka, A.; Jarockyte, G.; Ger, M.; Kuciauskas, D.; Kaupinis, A.; Valius, M.; Rotomskis, R.; Vetrone, F.; Karabanovas, V. Uptake of Upconverting Nanoparticles by Breast Cancer Cells: Surface Coating versus the Protein Corona. *ACS Appl. Mater. Interfaces* **2021**, *13* (33), 39076–39087.
- (21) Pan, J.-A.; Wu, H.; Gomez, A.; Ondry, J. C.; Portner, J.; Cho, W.; Hinkle, A.; Wang, D.; Talapin, D. V. Ligand-Free Direct Optical Lithography of Bare Colloidal Nanocrystals via Photo-Oxidation of Surface Ions with Porosity Control. ACS Nano 2022, 16 (10), 16067–16076.
- (22) Fischer, S.; Bronstein, N. D.; Swabeck, J. K.; Chan, E. M.; Alivisatos, A. P. Precise Tuning of Surface Quenching for Luminescence Enhancement in Core—Shell Lanthanide-Doped Nanocrystals. *Nano Lett.* **2016**, *16* (11), 7241—7247.
- (23) Kwock, K. W. C.; Lee, C.; Teitelboim, A.; Liu, Y.; Yao, K.; Alam, S. B.; Cohen, B. E.; Chan, E. M.; Schuck, P. J. Surface-Sensitive Photon Avalanche Behavior Revealed by Single-Avalanching-Nanoparticle Imaging. *J. Phys. Chem. C* **2021**, *125* (43), 23976–23982.
- (24) Hudry, D.; De Backer, A.; Popescu, R.; Busko, D.; Howard, I. A.; Bals, S.; Zhang, Y.; Pedrazo-Tardajos, A.; Van Aert, S.; Gerthsen, D.; Altantzis, T.; Richards, B. S. Interface Pattern Engineering in Core-Shell Upconverting Nanocrystals: Shedding Light on Critical Parameters and Consequences for the Photoluminescence Properties. *Small* **2021**, *17* (47), 2104441.
- (25) Marin, R.; Labrador-Paéz, L.; Skripka, A.; Haro-González, P.; Benayas, A.; Canton, P.; Jaque, D.; Vetrone, F. Upconverting Nanoparticle to Quantum Dot Förster Resonance Energy Transfer: Increasing the Efficiency through Donor Design. *ACS Photonics* **2018**, 5 (6), 2261–2270.
- (26) Pini, F.; Francés-Soriano, L.; Andrigo, V.; Natile, M. M.; Hildebrandt, N. Optimizing Upconversion Nanoparticles for FRET Biosensing. *ACS Nano* **2023**, *17* (5), 4971–4984.
- (27) Kotulska, A. M.; Pilch-Wróbel, A.; Lahtinen, S.; Soukka, T.; Bednarkiewicz, A. Upconversion FRET Quantitation: The Role of Donor Photoexcitation Mode and Compositional Architecture on the Decay and Intensity Based Responses. *Light Sci. Appl.* **2022**, *11* (1), 256.